Magnetic gates and guides for superconducting vortices

V. K. Vlasko-Vlasov, F. Colauto, A. I. Buzdin, D. Rosenmann, T. Benseman, and W.-K. Kwok

Phys. Rev. B **95**, 144504 — Published 4 April 2017

DOI: 10.1103/PhysRevB.95.144504

Magnetic gates and guides for superconducting vortices

V. K. Vlasko-Vlasov[1], F. Colauto[1,2], A. I. Buzdin[3] , D. Rosenmann[1], T. Benseman[1,4] , W.-K. Kwok[1]

[1] Argonne National Laboratory, 9700 South Cass Avenue, Argonne, Illinois 60439, USA
[2] Departamento de Fisica, Universidade Federal de Sao Carlos, 13565-905, Sao Carlos, SP, Brazil
[3] University Bordeaux , LOMA UMR- CNRS 5798, F-33405 Talence Cedex, France
[4] City University of New York,CUNY Queens College, Queens, NY 11367, USA

Epigraph: *It is better to see once than to assume 100 times*

We image the motion of superconducting vortices in niobium film covered with a regular array of thin permalloy stripes. By altering the magnetization orientation in the stripes using a small in-plane magnetic field, we can tune the strength of interactions between vortices and the stripe edges, enabling acceleration or retardation of the superconducting vortices in the sample and consequently introducing strong tunable anisotropy into the vortex dynamics. We discuss our observations in terms of the attraction/repulsion between point magnetic charges carried by vortices and lines of magnetic charges at the stripe edges, and derive analytical formulas for the vortex-magnetic stripes coupling. Our approach demonstrates the analogy between the vortex motion regulated by the magnetic stripe array and electric carrier flow in gated semiconducting devices. Scaling down the geometrical features of the proposed design may enable controlled manipulation of single vortices, paving the way for Abrikosov vortex microcircuits and memories.

Introduction

It is clearly recognized that power dissipation is a major issue in contemporary high density semiconductor microcircuits for computers and communication technologies. In this regard, superconducting single flux quantum devices [1-7] provide a route towards novel digital microelectronics. Such cryo-devices based on superconducting elements with minute losses offer superior performance in speed and exceptionally low power consumption. They operate with magnetic vortices, each carrying a single magnetic flux quantum [8] that can perform as natural 'bits' for digital operations. The notion of utilizing superconducting vortices in digital microprocessors and memories have been discussed for a while (see references in [1-7]). However, presently their technical realization is still in the research and development stage. Most of the efforts in vortex technology, termed *fluxtronics*, are devoted to the design and study of Josephson vortex circuits, where single flux quantum functionality is achieved by fine tuning assemblies of Josephson junctions (see e.g. [5]). Meanwhile, the alternative of constructing circuits based on single Abrikosov vortices remains largely unexplored. The idea of such devices was first suggested in the 1980's [9-14] and was revisited recently by the Stockholm group [7]. A number of proposed fluxonic devices relied on tunable trapping and translation of vortices in superconducting films with arrays of nanoholes of different shapes and symmetries [15-33]. Extensive citations on the subject can be found in [34]. These studies showed that it is possible to strongly enhance vortex pinning at integer and fractional matching fields, to induce guided motion of vortices, to realize vortex ratcheting or diode effects, and to synchronize vortex dynamics in ac fields.

Some of these works used small magnetic dots or ferromagnetic (FM) layers with domains in close proximity to a superconducting film to manipulate the superconducting (SC) transition temperature, T_c, and vortex dynamics. The micro and nano-patterning of the FM layer allowed various designs where superconducting channels can exist between normal regions, in which T_c was suppressed by the stray fields of the FM structures. For example, it was possible to create SC channels along domain walls between normal state regions formed under FM domains (so-called domain wall superconductivity [35-36]), and subsequently expand these channels by countering the stray fields effect in the FM domains with an external field. Furthermore, guided vortex motion can be generated [37, 30] with arrays of in-plane polarized magnetic nanobars, where the stray fields emanating from their ends produce weak channels of suppressed order parameter in the SC layer. Alternatively, magnetic arrays can provide strong, temperature independent magnetic pinning of vortices. For example, FM dots with perpendicular magnetic moments, **M,** can act as dipoles**,** attracting vortices polarized along the same direction towards their center while positioning oppositely polarized vortices at the dot's periphery, where the stray fields are aligned against **M**. For in-plane magnetized FM dots, there will be a dipolar potential with attraction and repulsion maxima for vortices located on opposite sides of the dot in the direction of **M**. Arrays of asymmetric magnetic dots (e.g. triangular) will form asymmetric potentials and thus assist unidirectional vortex motion along the asymmetry axis [18].

Early investigations of periodically patterned superconducting films and hybrid FM/SC structures were pioneered by the groups of Pannetier [38- 39], Bruynseraede and Moshchalkov [40- 41], Schuller and Vicent [42- 44], and theoretically supported by works of Lyuksyutov and Pokrovky [45-47], Peeters and Milosevic [48-52], Nori, Reichhardt and Olson [53-59], and Carneiro [60-65] with collaborators. Together with more recent works, these studies demonstrated the high potential for vortex manipulation with magnetic structures. A broad analysis of the vortex dynamics in FM/SC hybrids is presented in a number of comprehensive reviews [66-68] describing the basic effects and the underlying physics. References to the latest works on the subject can be found in [69-73].

Our group also contributed to the studies of different hybrid structures, including bilayers of SC/FM films containing magnetic stripe domains [74-77] and lithographically patterned FM strips with in-plane magnetization on top of a SC film [78]. We showed that FM stripe domains and the edges of FM strips could be used to guide vortices along them and serve as barriers for vortex motion across them. In our recent work, [79] we demonstrated that an array of *closely spaced* soft magnetic strips could allow triode-like control of Abrikosov vortices. By rotating the magnetization **M** of the stripes using relatively small in-plane fields, the magnetic charge responsible for the stray fields at the strip edges, can be easily tailored from zero (at **M**||edge) to a maximum (at **M**⊥edge). Consequently, the strip edges can become easy channels or barriers for vortex motion. The strength of the barrier and flux channeling effects are both defined by the orientation of **M** with respect to the stripe edges and by the magnitude of |**M**|. In this paper, we extend our work to samples with *larger inter-strip* gaps, which allows us to reveal flux distributions at oppositely polarized strip edges and to image and analyze fine details of the vortex dynamics. We show that the main guidance and pinning effects occur at stripe edges with the same magnetic charge polarity as that of entering vortices generated by an applied normal field, while the effect of oppositely charged edges is very weak.

Experiment and discussion

(a) Sample preparation

The sample is a 2x2mm^2 square of 100 nm SC Nb film (T_c =8.7K) with parallel FM permalloy (Py) stripes deposited on top. Both Nb and Py films were sputtered using a high-vacuum dc magnetron system. The Nb square was defined on oxidized Si substrate by laser lithography, and after sputtering and lift-off, covered with 15 nm SiO_2 layer to avoid proximity effects. Subsequently, an array of 35 μm wide and 40nm thick Py stripes with 5 μm gaps was fabricated on top of the Nb square, 200 μm away from the square edges using e-beam lithography and a lift-off process. An optical image of the sample is shown in Fig.1a.

The sample was covered with a garnet indicator film and placed on the cold finger of a closed cycle optical cryostat (Montana Instruments). Observations of the normal flux patterns at temperatures, T, ranging from 3.5 to 8.5K were performed with a polarized light microscope using a magneto-optical imaging technique [80]. The sample was cooled to a fixed T< T_c in the presence of a relatively small (20-150 Oe) in-plane field $H_{||}$, oriented at different angles with respect to the stripes in order to polarize the Py stripes. In the described experiments $H_{||}$ remained unchanged after cooling, securing the stripe polarization. We checked that in-plane fields up-to 1 kOe do not modify the normal flux dynamics in the reference 100 nm Nb film [81]. Background images revealing the stray fields at the edges of the Py stripes, which depend on the stripe polarization, were taken before application of the normal (perpendicular to the Nb film surface) field H_Z. These images were then subtracted from the images taken with the applied normal field such that only new vortices generated by H_z would be displayed. Below, we illustrate the main features of the dynamics of the entering H_z-vortices in the presence of transversely ($H_{||}$ along to the stripe width), longitudinally ($H_{||}$ along to the stripe length), and diagonally ($H_{||}$ at 45^0 to the stripe pattern) polarized Py stripes.

(b) Transverse polarization of Py stripes

Our thin Py stripes have the preferred magnetization direction in the film plane, negligible in-plane anisotropy, and a small coercivity. When an in-plane magnetic field of a few tens of Oersted is applied across the stripes, their magnetic moments **M** orient parallel with the field and form strongly localized magnetic charges along the long edges of the stripes (Fig.1b). The magnetic charge density is defined by the divergence of the magnetization near the stripe edge, ρ_M= - div**M**. For stripes with rectangular cross-section, ρ_M is proportional to the magnetization component M_n perpendicular to the edge face yielding surface charge density σ_M= M_n . Since the Py strip thickness, d_f = 40nm, is much smaller than the stripe and gap width (W=35 μm and G=5 μm respectively), we can consider each stripe edge as a magnetically charged filament with a linear charge density $M_n d_f$. The interaction of this linear charged edge with Abrikosov vortices, which can be described as point monopoles carrying magnetic charges of two flux quanta[1] $2\Phi_0$ [82], is analogous to the interaction between an

[1] A point charge in vacuum generates fields in the 4π spatial angle. However, the effective charge of the vortex at the SC surface produces the field only in half-space outside the SC. Therefore, the vortex "monopole" charge appears as $2\Phi_0$.

electrically charged line and electric point charges. This analogy allows a straightforward intuitive analysis of the vortex behavior in our hybrid structure as described below.

The magnetic charges produce alternating magnetic stray fields, H_s, at the Py stripe edges as revealed in Fig.1c by the bright and dark contrast in the MO image. The dark and bright contrast depict down and up directions of H_s, respectivitly, and corresponds to the sign of the magnetic charge at each stripe edge. In the following illustrations, these H_s generated MO patterns will be subtracted from images obtained with an additional *applied* normal-to-surface field, Hz, to reveal only vortex evolution generated by this field .

Small *normal* fields applied to thin SC films and plates are screened by a Meissner current, which induces concentrated H_z fields at the perimeter of our square Nb film visualized as bright contrast along the rim of the sample. With increasing H_z, Abrikosov vortices enter the film from all four sides of the sample in the shape of light flux lobes caused by defects and fractal flux dynamics (see [83] and refs. there) in conditions of strongly nonlinear supercurrent flow [84]. They overlap and form a pillow-shaped flux front as shown in Fig.2a. At larger H_z, the flux front advances inside the sample, arrives at the edges of the Py stripes, and start moving with different rates along and across the stripes resulting in an anisotropic pattern shown in (Fig.2b-c). Namely, the vortices enter with a noticeable delay *perpendicular* to the long edges of the Py stripes and accumulate at the stripe edges forming bright lines of increased B_z along them near the left and right sides of the Py pattern (Fig.2c). Meanwhile, vortices easily enter and move deep inside the sample *along* the inter-stripe gaps, forming bright enhanced B_z lines clearly resolved near the top and bottom sides of the Py pattern in Figs.2b-c. With increasing H_z, the normal flux expands from the inter-stripe gap region into the area beneath the Py stripes forming a modulated critical state. The B_z flux fronts propagating along the Py stripes from the top and bottom sides, meet at the horizontal center line of the sample, while the slower flux fronts advancing from the left and right sides remain far from the center of the sample. The resulting global critical state, when vortices occupy the whole sample, is shown in Fig. 2d. The lines of dark contrast in Fig.2d-e depict loci of the maximum screening of Hz corresponding to sharp turns of the supercurrent trajectories (see schemes in Figs.2l-n). Angles of these sharp current turn (SCT) lines are defined by the anisotropy of the average critical currents (J_c) in appropriate areas. In the peripheral area devoid of the Py stripes (within 200 μm from the Nb film edges) the SCT lines travel along the diagonals of the square. However, in the area under the Py stripe pattern the SCT lines are angled to reflect the enhanced average current *along* the stripes, $J_c^{||}$, and reduced critical currents *across* the stripes, $J_c^{\perp}$. An estimate of the anisotropy ratio from Fig.2d yields $J_c^{||}/ J_c^{\perp}\sim 2.6$. When H_z is increased further, the MO picture remains qualitatively the same, although the anisotropy decreases as demonstrated by the shortening of the dark central horizontal line in the critical state envelope in Fig.2e ($J_c^{||}/ J_c^{\perp}\sim 1.9$). At even larger normal field, the anisotropy reduces only slightly from this value.

Ramping the field down from a maximum (in this case H_z^{max}= 276 Oe) inverts the critical currents and the dark MO lines corresponding to maximum screening transform into bright lines of maximum trapped B_z (Fig.2f). The envelope-like shape of the critical state pattern remains the same as in the case for increasing H_z. With further decreasing field, the horizontal center line of the envelope lengthens, indicating the increased anisotropy of the critical currents at smaller B_z (Fig.2g). The decrease and increase of the anisotropy upon

ramping the field up and down, respectively, demonstrate the competition of inter-vortex interactions with the effect of the magnetic stripes.

Reducing H_z further causes negative flux (dark contrast) induced by the reversed currents to enter near the sample edges, and the critical state envelope shows a pronounced asymmetry with respect to the left and right sides of the stripe array (Fig.2h). The horizontal center line shifts to the left and the bright SCT lines on the left side of the Py pattern become shorter. Also a qualitative difference in the negative vortex entry is observed at the left and right sides of the sample. The asymmetry is better seen in the expanded view of the two sides upon both increasing and decreasing H_z in Fig.3. With increasing H_z (Fig.3a), the positive vortices are delayed at the first positively charged edge on the right, but pass easier across the furthest most left negatively charged edge and accumulate at the next positive edge (the left and right edges of the Py pattern are marked by double-arrows in Fig.3). Hence, positively charged stripe edges provide stronger pinning for positive H_z-vortices than negatively charged edges. Such a behavior is unusual because the maximum pinning force, F_p , for the oppositely charged edges should be practically the same. We associate the asymmetry with the dynamic nature of the vortex crossing over the stripe edges. When the positive vortex approaches the negatively charged line, it is attracted and accelerates towards the line. In contrast, a similar vortex approaching the positively charged line will decelerate and stop at the line.

With reducing H_z, the normal induction drops and changes sign around the most left edge of the Py pattern (contrast changes to dark) resulting in the increased local current along this edge. This yields a zigzag shift of the SCT line in the patterned area, as marked by the blue arrows in Fig.3b and schematically shown in Fig.3c. The average direction of the SCT lines under the stripes remains the same, but the triangular region bound by these lines on the left becomes smaller than that on the right. As a result, the centerline of the critical state envelope pattern extends to the left. At larger H_z, the left-right asymmetry disappears due to the increased vortex-vortex interactions overcoming the magnetic pinning. For opposite polarity of the transverse in-plane field, the asymmetric patterns mirror-flip horizontally.

Reducing the positive H_z field to zero and applying a negative H_z lead to advanced penetration of negative vortices along the Py stripes (Fig.2k), which eventually results in an anisotropic critical state similar to that in positive H_z (not shown). A new feature that emerges with increasing negative field is the unexpected appearance of extended negative vortex regions near the middle of the sample (dark streaks around the center line in Fig.2k) prior to their formation near the top and bottom stripe ends. These regions aligned with the stripes appear irregularly across the horizontal SCT line. We associate them with dynamic instabilities caused by the stripe-induced anisotropy of the vortex motion, which breaks the continuous loops of current flowing around the horizontal center-line of the sample. As a result, a chain of current loops appear supporting locally enhanced negative fields between them. The situation is similar to inversion of field between current rings of the same chirality. At larger negative fields, these negative vortex regions merge with streaks of negative B_z extending along the inter-stripe gaps from the top and bottom sides of the Py pattern, and form a structure similar to that observed with positive H_z. After ramping down the negative H_z, the positive vortices induced near the sample edges by the inverted critical currents are delayed stronger on the right side of the Py pattern but easily cross the left most stripe. Also,

the SCT center-line shifts to the right. The asymmetry is opposite to that observed for negative vortex entry when reducing positive H_z.

Fine details of vortex entry dynamics induced by transversely polarized Py stripes described above can be better seen in the MO images taken at larger magnification. Before the flux front induced by H_z reaches the tips of the Py stripes, brighter lines of positive B_z appear along the longitudinal stripe edges (marked by red vertical arrows and ellipse in Fig.4b). At the same time, dark spots of negative B_z emerge near the stripe ends (marked by tilted arrows and circle in Fig.4b). This unusual behavior is associated with vortices formed upon cooling the sample through T_c in the presence of stray fields (H_s) at the long Py stripe edges. As shown in the cross-section schematic of the sample in Fig.4, near the longitudinal Py edges with positive magnetic charge and diverging stray field H_s, the H_s-created vortices carry negative B_z. At the opposing longitudinal edge of the adjacent Py stripe with negative magnetic charge, the H_s-vortices carry positive B_z. When an external H_z is ramped up at $T<T_c$, the Meissner current induced Lorentz force F_L acts on the H_s-vortices in opposite directions. For positive H_s-vortices, F_L is pointing inside the sample while for negative H_s-vortices, F_L is directed towards the sample edges. When the B_z-front approaches the ends of the stripes, the Meissner current, J_M, ahead of the flux front becomes comparable with the critical current J_c flowing behind the front and F_L overcomes the pinning force. As a consequence, the positive H_s-vortices advance inside, while negative H_s-vortices move to the ends of the stripes where they assemble into dark droplets of negative B_z as illustrtaed in Fig. 4b. With further increasing field, incoming positive H_z-induced vortices annihilate these droplets and move into the inter-stripe gaps forming bright lines of enhanced positive B_z along them (Fig.4c). Also, the sharp B_z front enters in the shape of fingers across the uncharged ends of the Py stripes (indicated by arrows in Fig.4c). At higher fields, the modulated B_z-front advances inside the sample and forms an inhomogeneous distribution of B_z, where the density of vortices is maximum near the left sides of the gaps and smoothly decreases to the right (strips of bright contrast in Fig.4d). Thin lines in Fig.4d mark the middle of the inter-stripe gaps. Clearly, new positive H_z-vortices pile up on the left of the inter-stripe gaps at the positively charged stripe edges, but they pass more easily to the right across neighboring negatively charged stripe edges. This forms a flux gradient with B_z decaying rightward from the gap into the stripes. The above flux pattern corresponds to the wiggling current trajectories sharply bending near the positively charged edge of the Py stripes as sketched in Fig.5[2]. Here the increasing B_z corresponds to the downward arching and decreasing B_z to the upward arching of the current lines, and sharper bends in the current trajectory yield enhanced concentration of positive vortices at the positive edges. In Fig.5a the increasing distance between the current lines towards the top of the picture reflects the decay of the Meissner current towards the center of the sample. The meandering current trajectories yield spatially oscillating anisotropic supercurrent density.

---

[2] The qualitative current patterns in Fig.5a-b are constructed using following assumptions relevant for the SC plates and films in perpendicular fields. On average, the supercurrents flow along the sample edge and their direction corresponds to the partial screening of the increasing H_z. Distances between the current lines represent the inverse current density. The local enhancement (decrease) of B_z corresponds to the convex (concave) bending of the current lines, and the smaller bending radius yields stronger enhancement (decrease) of B_z. Within these assumptions the current patterns reproduce peculiarities of the B_z images.

The longitudinal current density ($J_{||}$ parallel to stripes) is maximum and the transverse current density ($J_{\perp}$ perpendicular to stripes) is minimum at the positively charged stripe edges. Towards the middle of the stripes $J_{||}$ drops and $J_{\perp}$ increases. The resulting SCT lines in the global critical state also meander, but straighten with increasing H_z.

The described flux evolution, in the presence of the transversely polarized Py stripes, is a consequence of the interactions between entering H_z–vortices induced by the applied normal field and the magnetic potential formed at the edges of the stripes. In the beginning these interactions are modified by the presence of field cooled H_s-vortices. As already mentioned, we can consider edges of the thin Py stripes polarized across their length as magnetically charged filaments. Positive and negative charge signs on opposite sides of the strip should form a potential barrier ridge and a potential valley groove for the positive H_z-vortices as shown in Fig.6. For long line with a linear charge density $\rho_l = \pm M d_f$, the magnetic field is directed radially from the line and decays as $H_s = \rho_l/2\pi R$ with radius R about the line. This approximation is valid when the length of the line is much larger than all other dimensions in the problem. Then for a normal vortex evaluated as a point magnetic charge of $2\Phi_0$ [82], the charged stripe edge will form a linear potential $U = \pm \int 2\Phi_0 H_s dx$ for vortex motion across the edge, logarithmically decaying with R. The spatial variations of the potential $U \sim \ln R$ and appropriate pinning forces $F_p \sim 1/R$ (in arbitrary units) in the gap area between the Py stripes are shown in Fig.6. Here the divergence of U and F_p at small distances is eliminated by a cut-off radius of the order of the FM film thickness. The large distance divergence of the logarithm cancels due to the opposite charges on either sides of the inter-stripe gaps.

Accurate calculations of the stripe edge-vortex coupling force with exact analytical formulas that account for the SC screening effects are discussed in the Appendix. They yield a magnetic pinning curve very close to that shown in Fig.6 at larger distances, but smoothed $F_P(R)$ close to the stripe edges due to supercurrents induced by H_s. In spite of this disparity, the simple analysis based on the interactions of linear and point magnetic charges yields a clear physical interpretation. Qualitatively similar description of magnetic pinning by FM microstructures was obtained within the London approximation for individual in-plane magnetized FM bars above a SC film in [51]. However, the integral formulas in [51] are dependent on the magnet bar shape, which is different from our geometry. In our case, long edges of the transversely polarized Py stripes introduce strong anisotropy to the critical currents with preferred current flow along the stripe edges. Such an anisotropy, responsible for the oscillating current patterns shown in Fig.5, is clearly revealed in our experiments (Figs.2-4).

(c) *Temperature variations of the vortex motion anisotropy induced by transversely polarized stripes*

In Fig.7 we present the global critical state pictures observed in the sample at different temperatures. As noted above, in the areas without magnetic stripes at the sample periphery, the SCT lines follow the square diagonals due to the isotropic currents in pure Nb film. In the area under the magnetic stripes the SCT lines change their direction and form envelope-like pattern corresponding to the critical current anisotropy. The ratio of the average currents along and across the stripes, $k = J_{c||}/J_{c\perp}$, depends on the applied normal field and changes with

temperature. Estimates of k(T) obtained from the MO patterns at smaller (squares) and larger H_z (circles) are presented in in Fig.8. At T>7K the positions of the SCT lines in the Py pattern area are not well defined and the values of k can be estimated only approximately. Fig.7 and 8 clearly show that the anisotropy increases with temperature. Such a behavior could be expected since at high temperatures the conventional vortex pinning by inherent defects decreases and the magnetic pinning by Py stripe edges becomes the dominant factor dictating vortex motion. At T<7K the error in the k-values is small and the plot shows that at least in this temperature range the anisotropy decreases at larger fields. This corresponds to the decreased efficiency of Py stripe induced magnetic pinning upon enhancement of intervortex interactions.

(d) *Longitudinal polarization of Py stripes*

For in-plane magnetic fields applied parallel to the stripe length, the magnetic charges are localized at the narrow stripe ends as shown in Fig.9. Small gaps between stripes are neutral, although there are decaying stray fields from the neighboring stripe ends. As before, we can consider the ends of the thin Py stripes, which are much longer than the film thickness, as filaments of positively and negatively charged magnetic monopoles. Therefore, they should form potential barrier ridges and potential valley grooves for H_z-vortex motion. However, unlike the transverse stripe polarization, inducing periodic potential lines all over the magnetic pattern, the longitudinal polarization of the stripes yields only two dashed potential lines (interrupted by the inter-stripe gaps) at the top and bottom edges of the patterned area. The sign of the charge at the stripe ends will define the vortex entry across them. Indeed, we observe accumulation of positive H_z-vortices at the positively charged stripe ends (dashed bright contrast near the bottom line of the stripe ends in Fig.9a-d and in the expanded view 9h) and unobstructed vortex entry across the negatively charged stripe ends at the top of the sample. At the bottom, the flux penetrates in the patterned area through the gaps between the positively charged ends. Here vortices enter in the shape of extended B_z balloons and vortex-free (dark) triangular regions remain behind the stripe ends (Fig. 9b and 9h). Although the depth of B_z penetration at the top and bottom of the sample appear to be practically identical, the total amount of vortices entering across the positively charged stripe ends is smaller than that passing through the negatively charged ends. This difference is more noticeable for narrower gaps between the stripes [79]. On the left and right neutral sides of the Py pattern the effect of the stripes is not visible.

With further increasing H_z, the normal flux penetrates deeper from all sides (Fig.9c). However, new vortices enter without a delay across the top (negative) and left and right (uncharged) edges of the Py pattern, where they form a smooth pillow-shaped front. The only barrier remains at the positively charged bottom strip ends, where the flux enters through the inter-stripe gaps and then spreads under neighboring stripes. Deeper into the sample, the extended vortex balloons coalesce into a smooth B_z front. New vortices accumulate near the external side of the positive strip ends leaving the small vortex density at their inner side as revealed by characteristic bright/dark diamonds in Fig.8b-c and 8k. At larger normal fields, when B_z occupies the entire sample and forms the global critical state, the SCT lines follow the square diagonals of the sample, indicating the absence of the average current anisotropy (Fig.9d). However, the darker/brighter diamonds (although with weaker contrast) still remain along the bottom Py stripe ends.

The contrast in the MO images inverts with subsequent ramp down of H_z. The exiting positive H_z-vortices now accumulate at the inner side of the positively charged stripe ends leaving a smaller B_z on the outer side, hence forming the inverted diamond patterns (Fig.9e and 9k). Finally, at H_z=0, balloons of negative vortices (dark) enter from the sample edges across the positive (bottom) ends of the Py stripes without obstruction (see green arrows in Fig. 9f).

At T> 6K the flux patterns in both increasing and decreasing normal fields reveal an apparent interaction between the longitudinally polarized Py stripes and the incoming and outgoing H_z induced vortices. Figures 10a-c show that with increasing H_z the flux streaks extend along the stripes and follow the stripe period. Minimum B_z position, separating the streaks, is settled along the middle-lines of the stripes. Maximum B_z forms along the inter-stripe gaps, indicating to the preferable propagation of the positive vortices along the gaps. This occurs at both top and bottom ends of the stripes even though the dark-bright diamonds appear only at the positive (bottom) stripe ends. Vortex motion across the stripes at the left and right sides of the stripe pattern remains basically unperturbed with a smooth B_z distribution absent of stripe periodicity. With decreasing H_z, the vortices preferentially exit the sample along the inter-stripe gaps, leaving behind bands of reduced B_z (Fig.10d-f). The observed flux periodicity indicates that at larger temperature, the coupling between the vortices and the Py stripes (probably due to weak polarization of Py by the vortex field) overcomes vortex pinning by inherent defects even when the long stripe edges are not magnetically charged. This coupling is also revealed by the appearance of the anisotropic envelope pattern in the global critical state. It is better visible in Fig.10e-f, where a short *vertical* SCT line appears at the center. It points to slightly smaller average currents *along* Py stripes, corresponding to easier vortex exit across the stripes towards their gaps along which they then exit to the sample edges. This anisotropy, though, is much smaller than that for the transversely polarized stripes.

(e) *Diagonally polarized Py stripes*

When the in-plane magnetic field is applied along the diagonal of the Py pattern, the magnetic charges, although smaller, appear along both the long sides and short ends of the stripes. Here, we observe both vortex guiding along the inter-stripe gaps and magnetic pinning at the positively charged stripe ends (Fig.11). However, both effects are weaker than for purely transverse and longitudinal stripe polarizations as described below.

In Fig.12 the H_z-vortex distributions are compared for transverse, diagonal, and longitudinal polarizations of the Py pattern at the same fixed normal field and temperature of H_z =15.4 Oe and T=4K, respectively. Qualitatively, the diagonally magnetized stripes act very similar to the transversely polarized stripes, although the penetration of B_z along the inter-stripe gaps (bright lines in Fig.12a-b) is shallower. Also, at the bottom stripe ends, there are dark/bright diamond structures as in the case for longitudinal polarization but with weaker contrast (i.e. with smaller B_z gradient).

In Fig.12d-f we compare the global critical state images at 4K for all three directions of $H_{||}$ at H_z =66.2 Oe. As expected, the envelope pattern shows smaller anisotropy for diagonal Py stripe polarization than for the perpendicular polarization.

The above observations show that vortex guided motion resulting from magnetic charges along the long stripe edges is the major effect of the Py stripe array. It produces the

largest dynamic anisotropy, which can be easily tuned by changing the angle of the in-plane field with respect to the magnetic stripes. In addition, at the ends of the Py stripes, it is possible to create a grid of strong pinning barriers regulating the entry of normal vortices through the inter-strip gaps. The barrier effect is maximum for longitudinal strip polarization, and also can be tuned by rotating the in-plane field from the long strip axis. Therefore it is possible to manipulate the normal vortex entry in the Py patterned area in a controllable way.

Conclusions

A parallel array of soft ferromagnetic (FM) stripes with in-plane magnetization on top of a superconducting film allows tunable manipulation of Abrikosov vortices. Extending our earlier finding [79], in this work we conducted a comprehensive study of the interactions between thin permalloy stripes and vortices in a Nb film and discussed the nature of the observed vortex guiding and magnetic pinning effects.

The main action of Py stripes on the underlying vortex dynamics is the control of vortex entry and exit in the sample. It arises from the magnetic charges emerging at the polarized stripe edges and is defined by their magnetization component perpendicular to the edge. Abrikosov vortices interact with these linear charges as positive or negative point-like magnetic monopoles depending on the vortex polarity. When the stripes are transversely magnetized by the in-plane field, positive and negative magnetic charges formed at opposite long edges create repulsive barrier ridge and attractive valley groove for the Abrikosov vortices. The strongly increasing magnetic potential at small distances from the lines of charged stripe edges (in the first approximation as lnR) causes a substantial supercurrent anisotropy. The anisotropy is strongly enhanced *locally* near the stripe edges and results in meandering current trajectories with sharp bends at the edges. It supports advanced penetration of vortices along the stripe edges of the same magnetic polarity and increased pinning for vortices moving across the edges. For vortices of the opposite magnetic polarity the stripe edges do not show a noticeable delay due to acceleration of vortices attracted towards such edges.

When the Py stripes are polarized longitudinally, their ends can work as a grid, where the gaps between the strips act as gates, while the ends themselves form an efficient barrier for Abrikosov vortices. Reducing the gap width provides stronger gating effect [79]. By rotating the magnetization of the Py strips with a relatively small in-plane field, the magnetic charges at their edges can be changed, which allows tuning the effects of the stripe pattern on the flux dynamics from vortex acceleration to inhibition.

We envision that by choosing appropriate material parameters (such as low pinning SC and soft FM components) and dimensions of the hybrid structure (thickness of SC and FM films, length and width of the stripes, and the size of the inter-stripe gap), it will be possible to fabricate components for controlling individual vortex motion for flux quantum electronics.

Acknowledgements

This work was supported by the U.S. Department of Energy, Office of Science, Materials Sciences and Engineering Division. The work of F. Colauto at Argonne National Laboratory was supported by the Sao Paulo Research Foundation FAPESP (grant No. 2015/06.085-3). We used sample manufacturing facilities of the Center for Nanoscale Materials, supported by the

U. S. DOE, Office of Science, Office of Basic Energy Sciences, under Contract No. DE-AC02-06CH11357. A.I.B. acknowledges support from French ANR projects “SUPERTRONICS”.

Appendix

Here we calculate the current in the SC film (in the XY-plane) induced by the edge of a long FM stripe (||Y), where magnetization is directed perpendicular to the edge face (**M**||X). This current multiplied by the flux quantum gives the Lorentz force acting on the Abrikosov vortex from the strip edge. The force is repulsive (“positive”) for the same sign of the magnetic charge of the vortex and the edge, and attractive (“negative”) for opposite magnetic charges. When the FM film thickness is much smaller than all other dimensions in the problem the magnetic field can be presented as a field of a linear monopole (long thin charged filament ||Y). It is directed radially perpendicular to the filament and decays with radius r as B=b/r. The magnetic charge per unit length in this case is $b=2Md_f$, where M is the saturation magnetization and d_f is the FM film thickness. The vector potential of the filament is $A_y=b\varphi$, where φ - is azimuthal angle around the filament axis. One can check that

$$rot\vec{A} = \hat{r}\left(\frac{1}{r}\frac{\partial A_y}{\partial \varphi}\right) + \hat{\varphi}\left(-\frac{\partial A_y}{\partial r}\right) = \hat{r}\frac{b}{r}$$

Below we use the Pearl’s approximation for thin SC films (d<λ) admitting a two-dimensional distribution of sheet currents, $\vec{j}_s$, in the SC film. Then

$$rot\vec{B} = \frac{4\pi}{c}\vec{j}_s = -\frac{\vec{A}}{\lambda^2}\, d\delta(z)$$

The total vector potential and the magnetic field can be divided into components due to the magnetic monopole of the vortex $(\vec{A}_V, \vec{B}_V)$ and due to currents induced by the magnetic filament $(\vec{A}_s, \vec{B}_s)$:

$\vec{A} = \vec{A}_V + \vec{A}_s$ and $\vec{B} = \vec{B}_V + \vec{B}_s$

Then

$rot\vec{B} = \frac{4\pi}{c}\vec{j}_s = -\frac{\vec{A}}{\lambda^2}\, d\delta(z)$, $rot\vec{B}_V = 0 \rightarrow rot\vec{B}_s = -\frac{\vec{A}}{\lambda^2}\, d\delta(z) = \frac{-d}{\lambda^2}[\vec{A}_V(z=0) + \vec{A}_s(z=0)]$

$rot\vec{B}_s = -\nabla^2\vec{A}_s$, and after Fourier transformation:

$$-(q^2+k^2)A_s(q,k) = [A_M(q,z=0) + A_s(q,z=0)]\frac{1}{\lambda_{eff}}$$

with $\lambda_{eff} = \frac{\lambda^2}{d}$, $q=(q_x, q_y)$, and $k=k_z$.

Then skipping the index z=0, we write the relation for $A_M(q)$ and $A_s(q)$ as

$$A_s(q) = \int A_s(q,k)\frac{dk}{2\pi} = -\frac{A_M+A_s}{2\pi\lambda_{eff}}\int\frac{dk}{q^2+k^2} = -\frac{A_M+A_s}{2\lambda_{eff}q}$$

So that $A_s(q) = \frac{-A_M(q)}{1+2\lambda_{eff}q}$

Then current in the SC film is:

$$\vec{j}(q) = -\frac{c}{4\pi\lambda_{eff}}\left(\vec{A}_M + \vec{A}_s\right) = -\frac{c}{4\pi\lambda_{eff}}\frac{2\lambda_{eff}q}{1+2\lambda_{eff}q}\vec{A}_M = -\frac{c}{2\pi}\frac{q}{1+2\lambda_{eff}q}\vec{A}_M$$

Now we consider the gap between two magnetic stripes, where the fields are produced by two oppositely charged filaments at a distance w and at some height h above the superconductor (h~$d_f/2$). Using the azimuthal angle φ=arctg(x/d), the total vector potential A_M is:

$$A_y(x) = b[arctg\left(\frac{x}{h}\right) - arctg\left(\frac{x+w}{h}\right)]$$

Accounting that h is small, we replace arctg with a step function of height π, so that the Fourier transform of $A_y(x)$ becomes:

$$A_q^y = \pi b\int_0^W e^{iqx}\,dx = -\frac{\pi b}{iq}(1-e^{iqw})$$

Then the current distribution can be calculated as inverse Fourier Transform by substituting A_q^y in above formula for J_q

$$J(x) = \frac{1}{2\pi}\int_{-\infty}^{\infty} J_q e^{-iqx}\,dq = \frac{1}{2\pi}\int_0^{\infty}(J_q e^{-iqx} + J_{-q}e^{iqx})dq =$$

$$= \frac{b}{2}\frac{c}{2\pi}\int_0^{\infty}\frac{-i}{1+2q\lambda_{eff}}\{\left(1-e^{-iqW}\right)e^{-iqx} - (1-e^{+iqW})e^{+iqx}\}\mathrm{dq} =$$

$$= \frac{cb}{2\pi}\int_0^{\infty}\frac{sinq(x+w)-sinqx}{1+2q\lambda_{eff}}\,\mathrm{dq}$$

which after substitution: $2q\lambda_{eff} = \tilde{q}$, $\frac{x}{2\lambda_{eff}} = \tilde{x}$, $\frac{W}{2\lambda_{eff}} = \widetilde{W}$, becomes:

$$J(x) = \frac{cb}{4\pi\lambda_{eff}}\int_0^{\infty}\frac{sin\tilde{q}(\tilde{x}+\tilde{w})-sin\tilde{q}\tilde{x}}{1+\tilde{q}}\,\mathrm{d\tilde{q}}$$

We define function $f(x) = \int_0^{\infty}\frac{sinqx}{1+q}\mathrm{dq} = Ci(x)sinx - Si(x)cosx + \frac{\pi}{2}cosx$

where $Ci(x) = -\int_x^{\infty}\frac{cost}{t}\mathrm{dt}$ is the cosine integral and $Si(x) = \int_0^x\frac{sint}{t}\mathrm{dt}$ is the sine integral.

Then $J(x) = \frac{cb}{4\pi\lambda_{eff}}[f(x+w) - f(x)]$

Asymptotically the cosine integral shows the logarithmic behavior for small arguments and saturates at large x:

$Ci(x\to 0)$-> $\gamma + lnx$ ($\gamma = 0.5772$ is the Euler constant) , $while\ Ci(x\to\infty)\to 0$

The sine integral at small x tends to zero $Si(x\to 0)$-> 0 , and $Si(x\to\pm\infty)\to\pm\pi/2$

However, one has to carefully choose the branches of Ci(x) and Si(x) for the intermediate x, which otherwise can result in a strongly oscillating function.

References

[1] H. Toepfer, and T. Ortlepp , Design infrastructure for rapid single flux quantum circuits , Cryogenics **49**, 643 (2009).

[2] S. Anders, M.G. Blamire, F.-Im. Buchholz, D.-G. Crété, R. Cristiano, P. Febvre, L. Fritzsch, A. Herr, E. Il'ichev, J. Kohlmann, et al., European roadmap on superconductive electronics – status and perspectives, Physica C **470**, 2079 (2010).

[3] O. A. Mukhanov, Energy-Efficient Single Flux Quantum Technology, IEEE Trans. Appl. Supercond. **21**, 760 (2011).

[4] K. K. Likharev, Superconductor digital electronics, Physica C **482** , 6 (2012).

[5] J. Kunert, O. Brandel, S. Linzen, O. Wetzstein, H. Toepfer, T. Ortlepp, and H.-G. Meyer, Recent Developments in Superconductor Digital Electronics Technology at FLUXONICS Foundry, IEEE Trans. Appl. Supercond. **23** , 1101707 (2013).

[6] D. S. Holmes, A. L. Ripple, and M. A. Manheimer, Energy-Efficient Superconducting Computing—Power Budgets and Requirements, IEEE Trans. Appl. Supercond. **23** , 1701610 (2013).

[7] T. Golod, A. Iovan, and V. M. Krasnov, Single Abrikosov vortices as quantized information bits, Nat. Comm. **6**, 8628 (2015).

[8] A. A. Abrikosov, On the Magnetic Properties of Superconductors of the Second group, Sov. Phys. JETP **5**, 1174 (1957).

[9] A. F. Hebard and A. T. Fiory, A memory device utilizing the storage of Abrikosov vortices at an array of pinning sites in a superconducting film, AIP Conf. Proceed. **44**, 465 (1978).

[10] W. Bachtold, The vortex file: a proposal for a new application of type-II superconductivity, IEEE Trans. Magn. **15**, 558 (1979).

[11] S. Uehara and K. Nagata, Trapped vortex memory cells, Appl. Phys. Lett. **39**, 992 (1981).

[12] J. Parisi, R. P. Huebener, and B. Mühlemeier, Experimental study of a superconducting vortex-memory device, Appl. Phys. Lett. **40**, 907 (1982).

[13] J. Parisi and R. P. Huebener, A Superconducting Vortex-Memory System , IEEE Trans. Electron. Devices **31**, 310 (1984).

[14] K. Miyahara, M. Mukaida, and K. Hohkawa, Abrikosov vortex memory, *Appl. Phys. Lett.* **47**, 754-756 (1985); Abrikosov vortex memory with improved sensitivity and reduced write current levels, IEEE Trans. Magn. **23**, 875 (1987).

[15] J. F. Wambaugh, C. Reichhardt, C. J. Olson, F. Marchesoni, and F. Nori, Superconducting fluxon pumps and lenses, Phys. Rev. Lett. **83**, 5106 (1999).

[16] M. B. Hastings, C. J. Olson Reichhardt, and C. Reichhardt, Ratchet Cellular Automata, Phys. Rev. Lett. **90**, 247004 (2003).

[17] B. Y. Zhu, F. Marchesoni, V. V. Moshchalkov, and F. Nori, Controllable step motors and rectifiers of magnetic flux quanta using periodic arrays of asymmetric pinning defects, Phys. Rev. B **68**, 014514 (2003).

[18] J. E. Villegas, S. Savel'ev, F. Nori, E. M. Gonzalez, J. V. Anguita, R. Garcia, and J. L. Vicent, A superconducting reversible rectifier that controls the motion of magnetic flux quanta, Science **302**, 1188 (2003).

[19] M. Berciu, T. G. Rappoport, and B. Janko, Manipulating spin and charge in magnetic semiconductors using superconducting vortices, Nature **435**, 71 (2005).

[20] S. Ooi, S. Savel'ev, M. B. Gaifullin, T. Mochiku, K. Hirata, and F. Nori, Nonlinear Nanodevices Using Magnetic Flux Quanta, Phys. Rev. Lett. **99**, 207003 (2007).

[21] M. Milosevic, G. R. Berdiyorov, and F. M. Peeters, Fluxonic cellular automata, Appl. Phys. Lett. **91**, 212501 (2007).

[22] K. Yu, T. W. Heitmann, C. Song, M. P. DeFeo, B. L. T. Plourde, M. B. S. Hesselberth, and P. H. Kes, Asymmetric weak-pinning superconducting channels: Vortex ratchets, Phys. Rev. B **76** , 220507 (2007).

[23] W. Gillijns, A. V. Silhanek, V. V. Moshchalkov, C. J. O. Reichhardt, and C. Reichhardt, Origin of reversed vortex ratchet motion, Phys. Rev. Lett. **99**, 247002 (2007).

[24] N. Verellen, A. V. Silhanek, W. Gillijns, V. V. Moshchalkov, V. Metlushko, F. Gozzini, and B. Ilic, Switchable magnetic dipole induced guided vortex motion, Appl. Phys. Lett. **93**, 022507 (2008).

[25] A. Yu. Aladyshkin, J. V. de Vondel, C. C. D. Silva, and V. V. Moshchalkov, Tunable anisotropic nonlinearity in superconductors with asymmetric antidot array, Appl. Phys. Lett. **93** , 082501 (2008).

[26] R. Woerdenweber, E. Hollmann, J. Schubert, R. Kutzner, and A. K. Ghosh, Pattern induced phase transition of vortex motion in high-T-c films, Appl. Phys. Lett. **94** , 202501 (2009).

[27] J. F. He, N. Harada, T. Ishibashi, H. Naitou, and H. Asada, Magneto-Optical Observation of Anisotropic Critical Current Density in Nb Films with Artificial Asymmetric Pinning Potential, Jap. J. Appl. Phys. **48** , 063003 (2009).

[28] B. B. Jin, B. Y. Zhu, R. Wördenweber, C. C. de Souza Silva, P. H. Wu, and V. V. Moshchalkov, High-frequency vortex ratchet effect in a superconducting film with a nanoengineered array of asymmetric pinning sites, Phys. Rev. B **81**, 174505 (2010).

[29] A. V. Kapra, V. R. Misko, D. Y. Vodolazov, and F. M. Peeters, The guidance of vortex-antivortex pairs by in-plane magnetic dipoles in a superconducting finite-size film, SUST **24**, 024014 (2011).

[30] A. V. Kapra, V. R. Misko, and F. M. Peeters, Controlling magnetic flux motion by arrays of zigzag-arranged magnetic bars, SUST **26**, 025011 (2013).

[31] J. Trastoy, C. Ulysse, R. Bernard, M. Malnou, N. Bergeal, J. Lesueur, J. Briatico, and J.□E. Villegas, Tunable Flux-Matching Effects in High-Tc Superconductors with Nonuniform Pinning Arrays, Phys. Rev. Appl. **4**, 054003 (2015).

[32] J. del Valle, A. Gomez, E. M. Gonzalez, M. R. Osorio, D. Granados, and J. L. Vicent, Superconducting/magnetic Three-state Nanodevice for Memory and Reading Applications , Sci. Rep. **5**, 15210 (2015).

[33] O. V. Dobrovolskiy, M. Huth, and V. A. Shklovskij, Alternating current-driven microwave loss modulation in a fluxonic metamaterial, Appl. Phys. Lett. **107**, 162603 (2015).

[34] V. V. Moshchalkov and J. Fritzsche, Nanostructured Superconductors, World Scientific, Singapore (2011).

[35] A. Yu. Aladyshkin, A. I. Buzdin, A. A. Fraerman, A. S. Mel'nikov, D. A. Ryzhov, and A. V. Sokolov, Domain-wall superconductivity in hybrid superconductor-ferromagnet structures, Phys. Rev. B **68**, 184508 (2003).

[36] Z. R. Yang, M. Lange, A. Volodin, R. Szymczak, and V. V. Moshchalkov, Domain-wall superconductivity in superconductor-ferromagnet hybrids, Nat. Mater. **3**, 793-798 (2004).

[37] A. V. Silhanek, V. N. Gladilin, J. Van de Vondel, B. Raes, G. W. Ataklti, W. Gillijns, J. Tempere, J. T. Devreese, and V. V. Moshchalkov, Local probing of the vortex–antivortex dynamics in superconductor/ferromagnet hybrid structures, SUST **24**, 024007 (2011).

[38] O. Geoffroi, D. Givord, Y. Otani, B. Pannetier, F. Ossart, Magnetic and transport properties of ferromagnetic particulate arrays fabricated on superconducting thin-films, J. Magn. Magn. Mater. **121**, 223 (1993).

[39] Y. Otani, B. Pannetier, J. P. Nozieres, and D. Givord, Magnetostatic interactions between magnetic arrays and superconducting thin-films, J. Magn. Magn. Mater. **126**, 622 (1993).

[40] V. V. Metlushko, M. Baert, R. Jonckheere, V. V. Moshchalkov, and Y. Bruynseraede, Matching effects in Pb/Ge multilayers with the lattice of submicron holes, Sol. St. Commun. **91**, 331 (1994).

[41] M. Baert, V. V. Metlushko, R. Jonckheere, V. V. Moshchalkov, and Y. Bruynseraede, Composite flux-line lattices stabilized in superconducting films by a regular array of artificial defects, Phys. Rev. Lett. **74** , 3269 (1995).

[42] J. I. Martin, M. Velez, J. Nogues, and I. K. Schuller, Flux pinning in a superconductor by an array of submicrometer magnetic dots, Phys. Rev. Lett. **79** , 1929 (1997).

[43] Y. Jaccard, J. I. Martin, M. C. Cyrille, M. Velez, J. L. Vicent, and I. K. Schuller, Magnetic pinning of the vertex lattice by arrays of submicrometric dots, Phys. Rev. B **58** , 8232 (1998).

[44] J. L. Martin, M. Velez, A. Hoffmann, I. K. Schuller, and J. L. Vicent, Artificially induced reconfiguration of the vortex lattice by arrays of magnetic dots, Phys. Rev. Lett. **83** , 1022 (1999).

[45] I. F. Lyuksyutov and V. L. Pokrovsky, Magnetization Controlled Superconductivity in a Film with Magnetic Dots, Phys. Rev. Lett. **81**, 2344 (1998).

[46] I. F. Lyuksyutov and D. G. Naugle, Frozen flux superconductors, Mod. Phys. Lett. B **13** , 491 (1999).

[47] S. Erdin, A.F. Kayali, I.F. Lyuksyutov, and V.L. Pokrovsky, Interaction of mesoscopic magnetic textures with superconductors, Phys. Rev. B **66**, 014414 (2002).

[48] I. K. Marmorkos, A. Matulis, and F. M. Peeters, Vortex structure around a magnetic dot in planar superconductors, Phys. Rev. B **53**, 2677 (1996).

[49] M. V. Milosevic, S. V. Yampolskii, and F. M. Peeters, Magnetic pinning of vortices in a superconducting film: The (anti)vortex-magnetic dipole interaction energy in the London approximation, Phys. Rev. B **66**, 174519 (2002).

[50] M.V. Milosevic and F.M. Peeters, Interaction between a superconducting vortex and an out-of-plane magnetized ferromagnetic disk:
Influence of the magnet geometry, Phys. Rev. B **68**, 094510 (2003).

[51] M. V. Milosevic and F. M. Peeters, Vortex pinning in a superconducting film due to in-plane magnetized ferromagnets of different shapes: The London approximation, Phys. Rev. B **69**, 104522 (2004).

[52] M. V. Milosevic and F. M. Peeters, Vortex-antivortex nucleation in superconducting films with arrays of in-plane dipoles, Physica C **437-438**, 208 (2006).

[53] J. F. Wambaugh, C. Reichhardt, C. J. Olson, F. Marchesoni, and F. Nori, Superconducting fluxon pumps and lenses, Phys. Rev. Lett. **83**, 5106 (1999).

[54] C. J. Olson, C. Reichhardt, B. Janko, and F. Nori, Collective interaction-driven ratchet for transporting flux quanta, Phys. Rev. Lett. **87**, 177002 (2001).

[55] B. Y. Zhu, F. Marchesoni, V. V. Moshchalkov, and F. Nori, Controllable step motors and rectifiers of magnetic flux quanta using periodic arrays of asymmetric pinning defects, Phys. Rev. B **68**, 014514 (2003).

[56] M. B. Hastings, C. J. Olson Reichhardt, and C. Reichhardt, Ratchet Cellular Automata, Phys. Rev. Lett. **90** , 247004 (2003) .

[57] S. Ooi, S. Savel'ev, M. B. Gaifullin, T. Mochiku, K. Hirata, and F. Nori, Nonlinear Nanodevices Using Magnetic Flux Quanta, Phys. Rev. Lett. **99**, 207003 (2007).

[58] V. R. Misko, D. Bothner, M. Kemmler, R. Kleiner, D. Koelle, F. M. Peeters, and F. Nori, Enhancing the critical current in quasiperiodic pinning arrays below and above the matching magnetic flux, Phys. Rev. B **82**, 184512 (2010).

[59] V. R. Misko and F. Nori, Magnetic flux pinning in superconductors with hyperbolic-tesselation arrays of pinning sites, Phys. Rev. B **85**, 184506 (2012).

[60] C. C. de Souza Silva and G. Carneiro, Simple model for dynamical melting of moving vortex lattices interacting with periodic pinning, Phys. Rev. B **66**, 054514 (2002).

[61] C. C. de Souza Silva and G. Carneiro, Transverse pinning and vortex displacement fluctuations of moving vortex lattices interacting with periodic pinning, Physica C **391**, 203 (2003).

[62] G. Carneiro, Pinning and creation of vortices in superconducting films by a magnetic dipole, Phys. Rev. B **69**, 214504 (2004).

[63] G. Carneiro , Interaction between vortices in superconducting films and magnetic dipole arrays, Physica C **404**, 78 (2004).

[64] G. Carneiro, Tunable interactions between vortices and a magnetic dipole, Phys. Rev. B **72**, 144514 (2005).

[65] G. Carneiro, Tunable ratchet effects for vortices pinned by periodic magnetic dipole arrays, Physica C **432**, 206 (2005).

[66] I. F. Lyuksyutov and V. L. Pokrovsky, Ferromagnet/superconductor hybrids, Adv. Phys. **54**, 67 (2005).

[67] M. Velez, J. I. Martin, J. E. Villegas, A. Hoffman, E. M. González, J. L. Vicent, and I. K. Schuller, Superconducting vortex pinning with artificial magnetic nanostructures, J. Magn. Magn. Mater. **320**, 2547 (2008).

[68] A. Yu. Aladyshkin, A. V. Silhanek, W. Gillijns, and V. V. Moshchalkov, Nucleation of superconductivity and vortex matter in superconductor/ferromagnet hybrids, Supercond. Sci. Technol. **22**, 053001 (2009).

[69] J. Brisbois, O.–A. Adami, , J. I. Avila, M. Motta, W. A. Ortiz, N. D. Nguyen, P. Vanderbemden, B. Vanderheyden, R. B. G. Kramer, and A. V. Silhanek, Magnetic flux penetration in Nb superconducting films with lithographically defined microindentations, Phys. Rev. B **93** , 054521 (2016).

]70] C. Reichhardt and C. J. Olson Reichhardt, Transverse ac-driven and geometric ratchet effects for vortices in conformal crystal pinning arrays, Phys. Rev. B **93** , 064508 (2016).

[71] M. Trezza, C. Cirillo, A. L. Dolgiy, S. V. Redko, V. P. Bondarenko, A. V. Andreyenka, A. L. Danilyuk, S. L. Prischepa, and C. Attanasio, Change of the topology of a superconducting thin film electromagnetically coupled with an array of ferromagnetic nanowires, Supercond. Sci. Technol. **29** , 015011 (2016).

[72] O.V. Dobrovolskiy, Abrikosov fluxonics in washboard nanolandscapes, *Physica C (2016)*, http://dx.doi.org/10.1016/j.physc.2016.07.008

[73] Z. Adamus, M. Cieplak, M. Konczykowski, L. Y. Zhu, and C. L. Chien, Influence of magnetic domain landscape on the flux dynamics in superconductor/ ferromagnet bilayers, Phys. Rev. B **93** , 054509 (2016).

[74] V. Vlasko-Vlasov, U. Welp, G. Karapetrov, V. Novosad, D. Rosenmann, M. Iavarone, A. Belkin, and W. -K. Kwok, Guiding superconducting vortices with magnetic domain walls, Phys. Rev. B **77**, 134518 (2008).

[75] V. K. Vlasko-Vlasov, U. Welp, A. Imre, D. Rosenmann, J. Pearson, and W.-K. Kwok, Soft magnetic lithography and giant magnetoresistance in superconducting/ferromagnetic hybrids,Phys. Rev B **78** , 214511 (2008).

[76] V. Vlasko-Vlasov, U. Welp, W. Kwok, D. Rosenmann, H. Claus, A. I. Buzdin, and A. Melnikov, Coupled domain structures in superconductor/ferromagnet Nb-Fe/garnet bilayers, Phys. Rev B **82** , 100502 (2010).

[77] V. Vlasko-Vlasov, A. Buzdin, A. Melnikov, U. Welp, D. Rosenmann, L. Uspenskaya, V. Fratello, and W. Kwok, Domain structure and magnetic pinning in ferromagnetic/superconducting hybrids, Phys. Rev. B **85** , 064505 (2012).

[78] V. K. Vlasko-Vlasov, E. Palacios, D. Rosenmann, J. Pearson, Y. Jia, Y. L. Wang, U. Welp, and W.-K. Kwok, Self-healing patterns in ferromagnetic-superconducting hybrids, Supercond. Sci. Technol. **28** , 035006 (2015).

[79] V. K. Vlasko-Vlasov, F. Colauto, T. Benseman, D. Rosenmann, and W.-K. Kwok, Triode for Magnetic Flux Quanta, Sci. Rep. | 6:36847 | DOI: 10.1038/srep36847

[80] V. K. Vlasko-Vlasov, G. W. Crabtree, U. Welp, and V. I. Nikitenko, Magneto-optical studies of magnetization processes in high-Tc superconductors, NATO ASI Ser., Ser. E **356**, 205-237 (1999).

[81] V. K. Vlasko-Vlasov, F. Colauto, A. I. Buzdin, D. Carmo, A. M. H. Andrade, A. A. M. Oliveira, W. A. Ortiz, D. Rosenmann, and W.-K. Kwok, Crossing fields in thin films of isotropic superconductors, Phys. Rev. B **94**, 184502 (2016).

[82] G. Carneiro and E. H. Brandt, Vortex lines in films: Fields and interactions, Phys. Rev. B **61**, 6370 (2000).

[83] V. K. Vlasko-Vlasov, U. Welp, V. Metlushko, and G. W. Crabtree, Experimental test of the self-organized criticality of vortices in superconductors, Phys. Rev. B **69**, 140504R (2004).

[84] M. Friesen and A. Gurevich, Nonlinear current flow in superconductors with restricted geometries, Phys. Rev. B **63**, 064521 (2001).

Figures

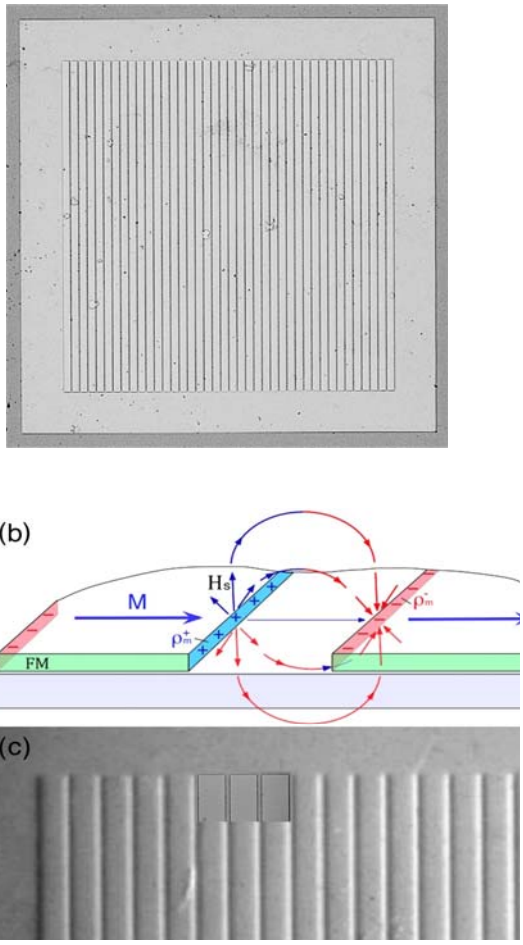

Fig.1 (a)-Optical picture of 2x2 mm Nb square with Py stripes in the middle. (b)-Schematic of magnetic charges along the long edges of transversely polarized Py stripes. Each edge forms a magnetic monopole line with radially diverging magnetic stray fields H_s. (c) Magneto-optical image of the stray fields induced by the array of transversely polarized Py stripes. Bright and dark contrast indicate Up and Down direction of H_s. The overlayed rectangle in (c) shows the positions of the stripe ends and gaps.

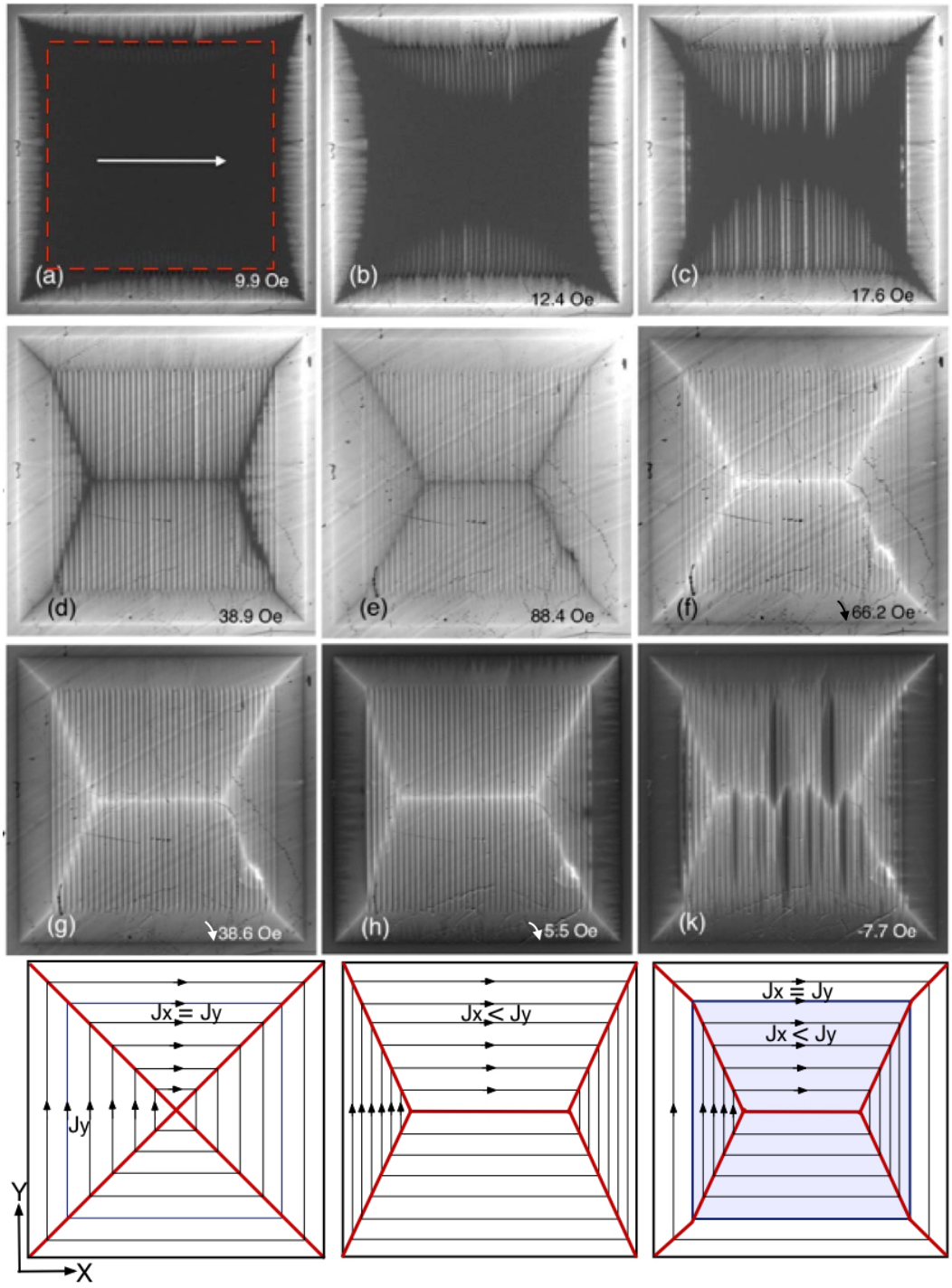

(l) (m) (n)

Fig.2 Magneto-optical images of the normal flux distribution in the sample with transversely polarized stripes. T=4K . Direction of $H_{||}$ is shown by arrow in (a). Dashed square in (a) outlines area of the Py pattern. The applied normal field H_z increases in (a)-(e), decreases in (f)-(h), and changes sign in (k). Values of Hz are shown on the panels. Intensity of bright contrast corresponds to the density of positive H_z-vortices. Dark contrast at the sample edges in (h)-(k) and along the stripes in (k) reveals negative B_z. Current schemes at the bottom correspond to isotropic (l) and anisotropic (m) homogeneous samples, and sample with anisotropic middle part (n). In the presented

geometrical model of the critical state (l-n) distances between the supercurrent lines are inversely proportional to the current density. The angle of the SCT lines, where maximum screening occurs in the increasing Hz (dark lines in d-e) or maximum trapped flux remains in the decreasing Hz (bright lines in f-h), is defined by the ratio of J_x/J_y.

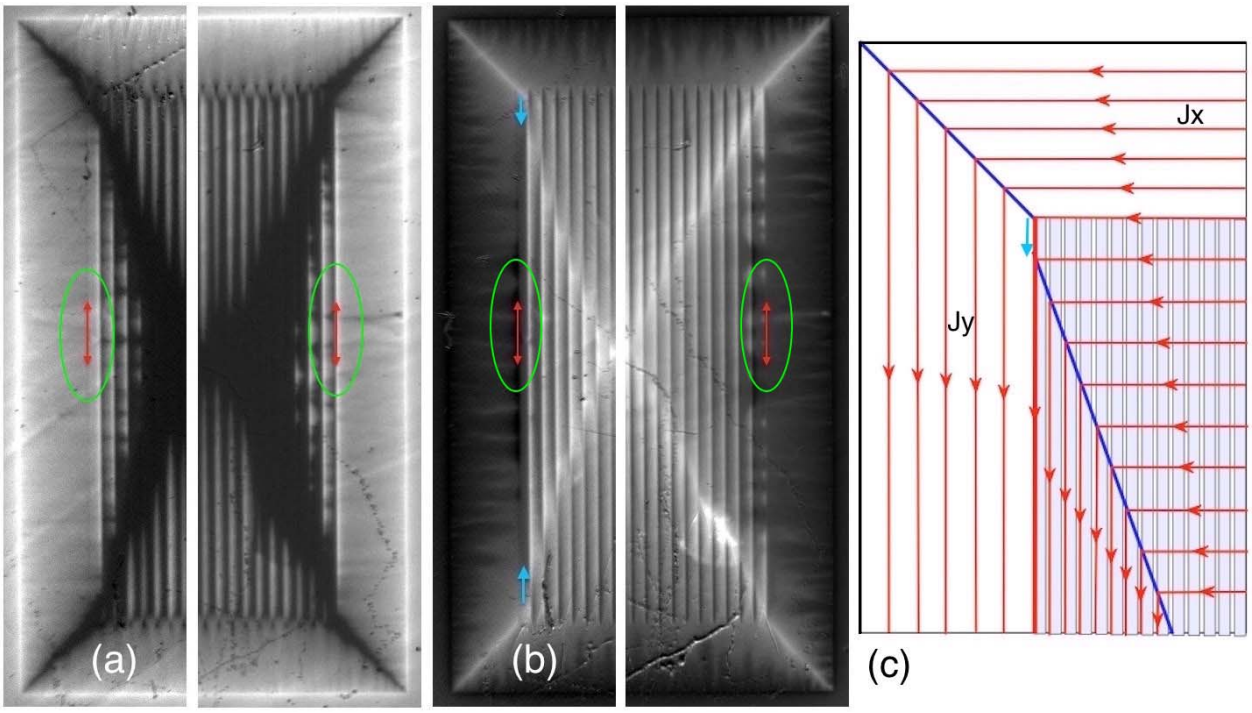

Fig.3 Left-right asymmetry of the vortex patterns for transversely polarized Py stripes. The left and right sides of the sample at 4K in increasing (a, H_z=23.8 Oe) and decreasing field (b, H_z = 0 after H_z^{max}=276 Oe). The furthest most left and right edges of the Py magnetic stripes are marked by red double-arrows. The shift of the bright SCT lines on the left side in (b) is shown by blue arrows. Positive vortices (bright) are not pinned at the most left stripe edge in (a) (see left ellipse), but negative vortices (dark) are impeded at this edge in (b). Vice versa, positive vortices are delayed and accumulated at the most right edge in (a) (right ellipse) but negative vortices move across it smoothly in (b). (c)- Schematic explaining the zigzag shift of the SCT line in (b) due to enhanced J_c along the left side of the magnetic pattern. Similar but smaller zigzag shifts appear at each inter-stripe gap (not shown on the schematic but revealed on zigzagging SCT lines in (b)).

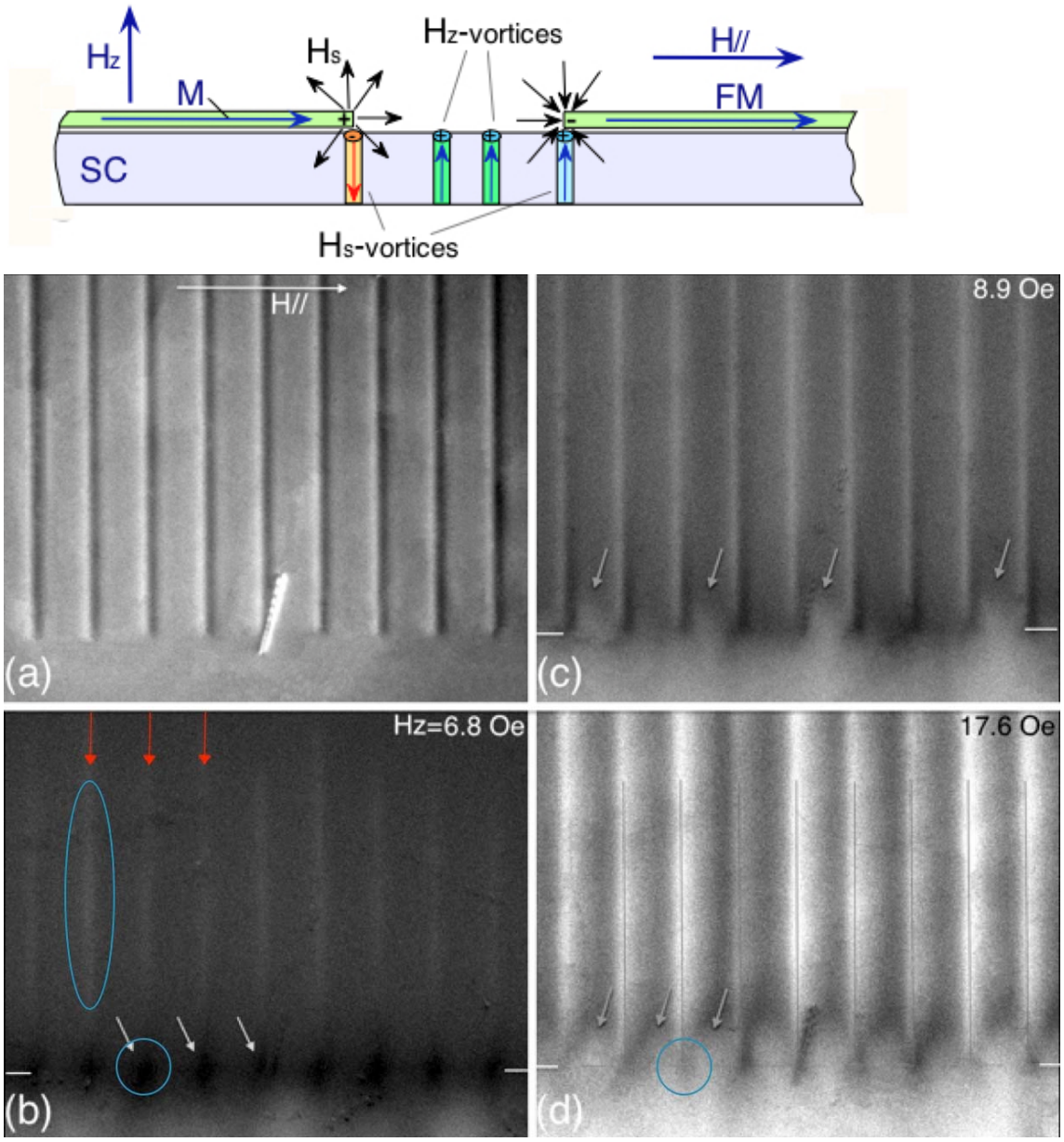

Fig.4 Expanded view of the normal flux entry at small H_z near bottom ends of the stripes. Schematic of stray fields H_s (top) and bright/dark contrast in (a) show Up and Down components of H_s due to the transversely polarized Py stripes at H_z=0. This contrast is subtracted from other MO images to reveal entering H_z- vortices. T=5K, field values are shown on the panels. Short horizontal lines in (b)-(d) mark the position of stripe ends. Tilted arrows in (b) (one encircled) mark dark spots of negative B_z due to the downward motion of negative H_s-vortices. Brighter contrast along the stripe edges in (b)-(d) reveals the advanced guided motion of the positive Abrikosov vortices (marked by vertical arrows and by ellipse in (b)). Arrows in (c)-(d) point to the fingers of the secondary positive B_z front entering across the stripe ends. Thin vertical lines in (d) mark the middle of the inter-stripe gaps. Circle in (d) marks lower B_z spot near stripe corners.

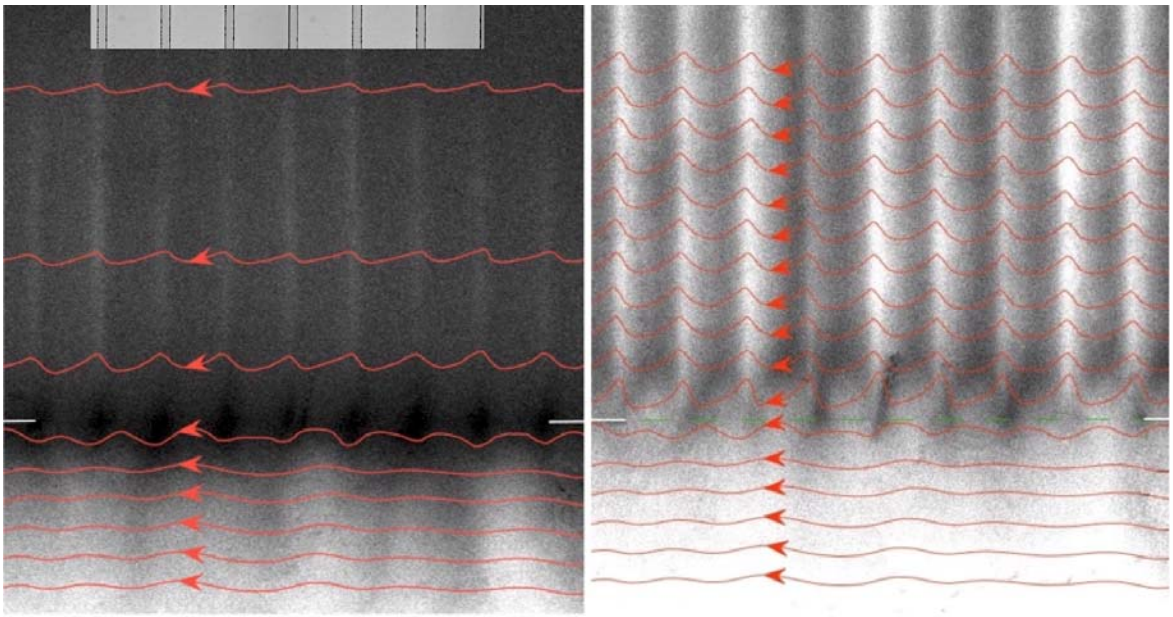

Fig5 Current trajectories (red lines) for the flux patterns in Fig.4(b) and 4(d). Left-top insert shows position of the stripe gaps.

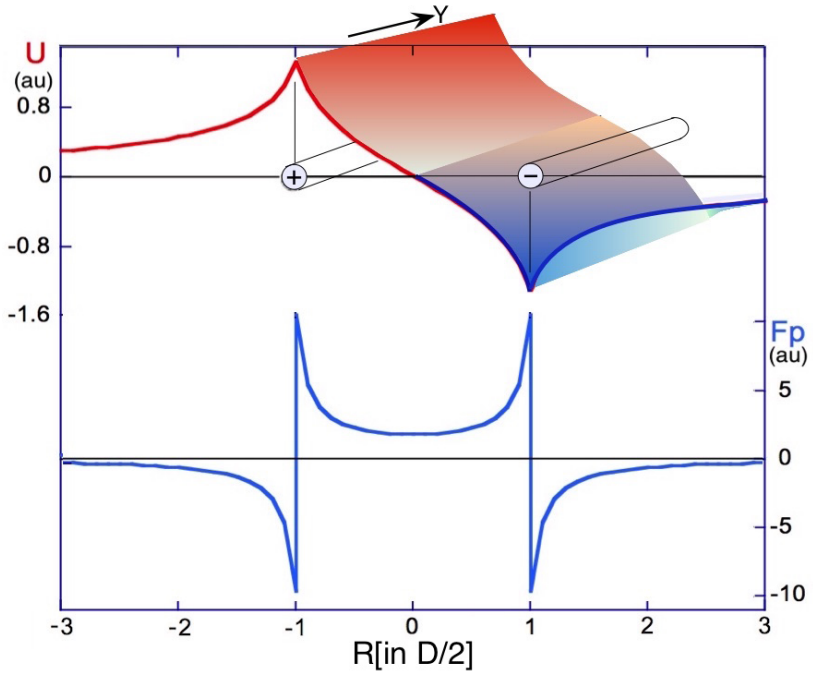

Fig.6 The magnetic potential U~lnR (top) and magnetic pinning force F_p~1/R (bottom) for Abrikosov vortices moving across the gap between thin long transversely polarized FM stripes. U and F_p are in arbitrary units, and the distance R is in units of half-the gap (D/2) between the stripes. Potential barrier ridge and potential valley groove are formed along positively and negatively charged edges respectively (|| Y).

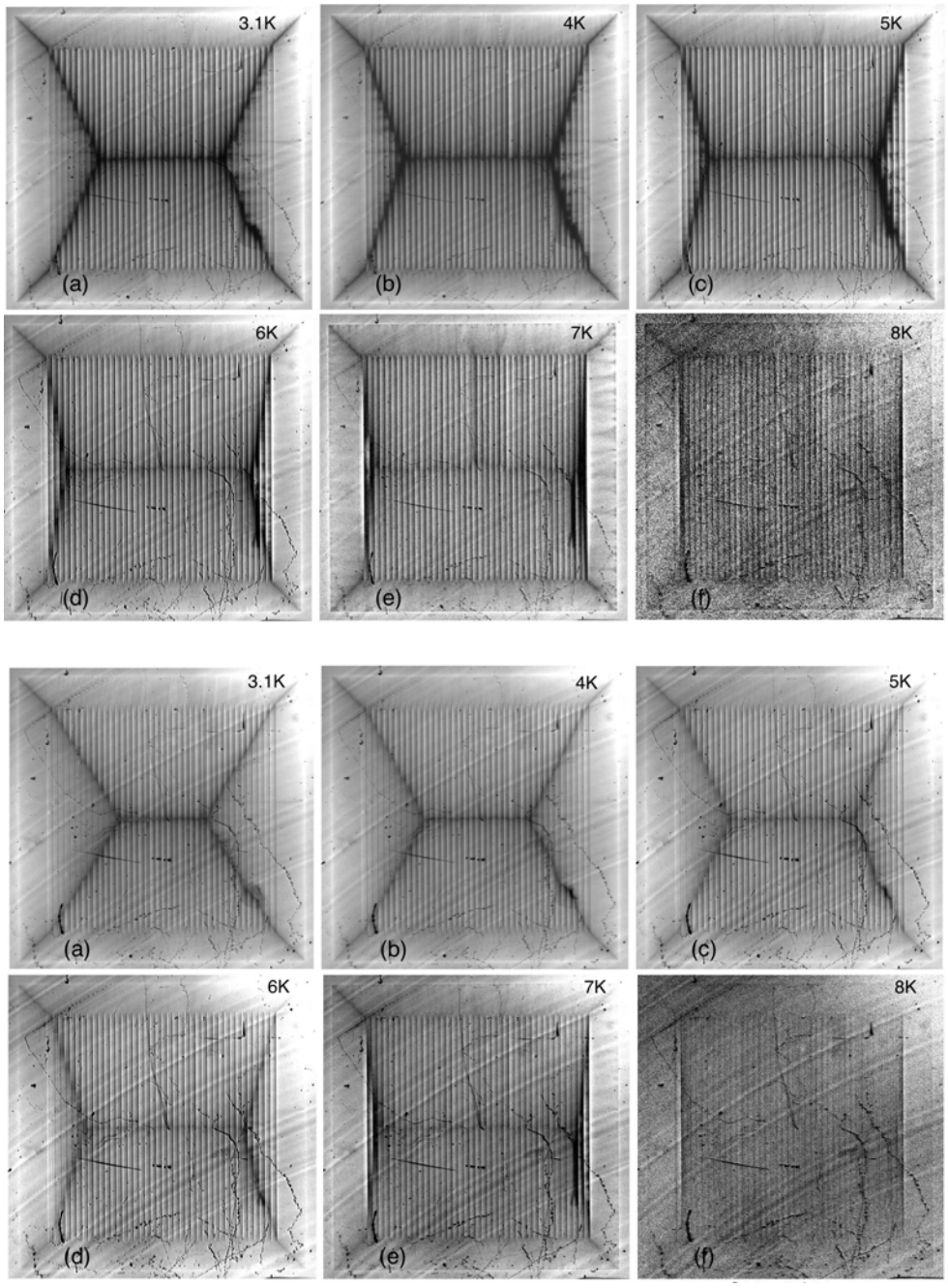

Fig.7 Temperature variations of anisotropic critical states for transversely polatized stripes at smaller field H_{fill} , when vortices first fill the entire sample (top set, H_{fill} decreases from 55 Oe to 5 Oe with increasing T from 3.1K to 8K), and at larger field (bottom set, H_z=110 Oe). The anisotropy increases with T and drops with H_z.

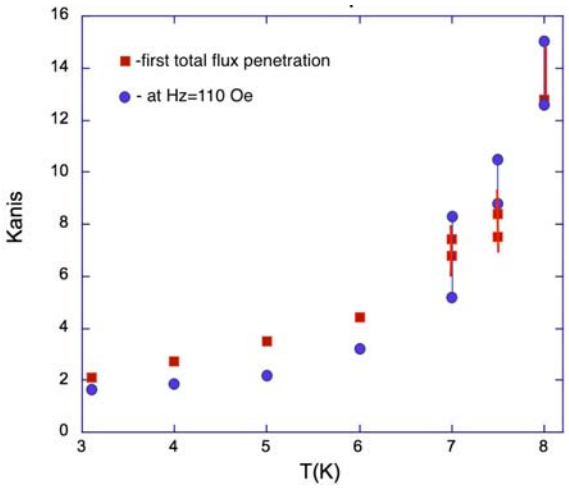

Fig.8 Ratio of the critical currents along and across transversely polarized Py stripes estimated from positions of SCT lines in MO patterns. At T>7K estimates are approximate and presented by double dots.

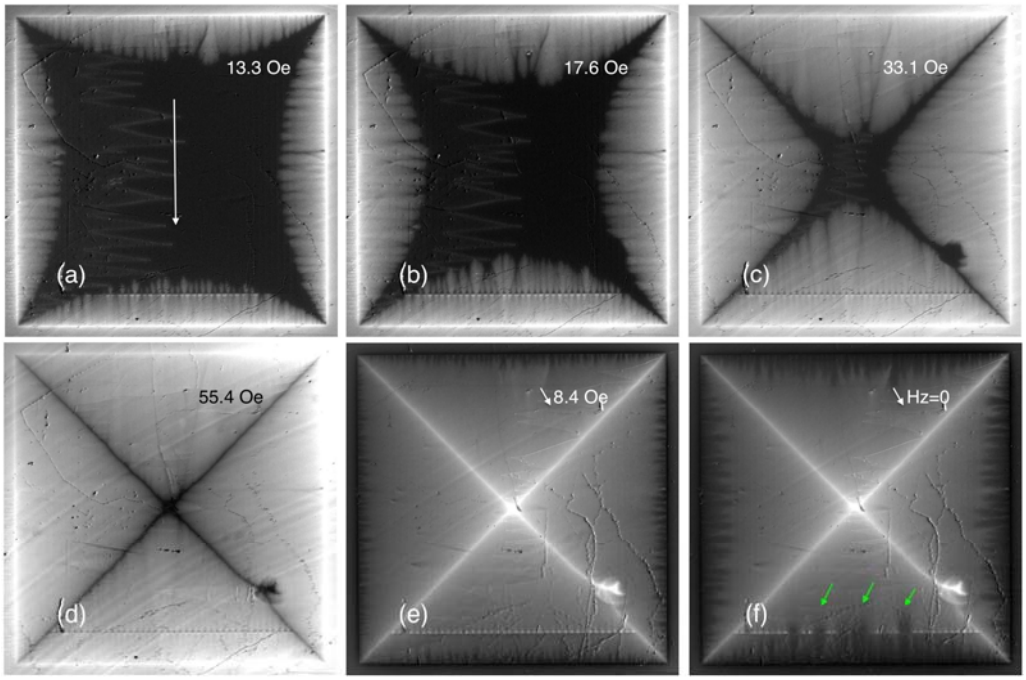

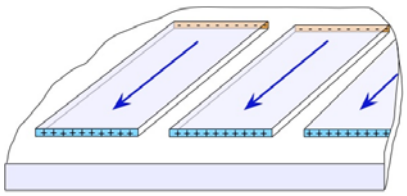

(g)

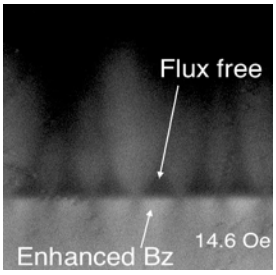

(h)

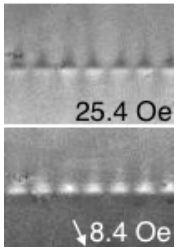

(k)

Fig.9 Normal flux in the sample with longitudinally polarized Py stripes in increasing (a)-(d) and decreasing (e)-(f) magnetic field H_z at T=4K. The direction of the in-plane field is shown in (a) by arrow. (g)- schematic of magnetic charges emerging at short ends of the stripes. (h)-expanded view of the vortex distribution near the bottom line of stripe ends at smaller H_z . (k)-inversion of the flux "rhombs" near positive stripe ends with increasing (top) and decreasing H_z (bottom).

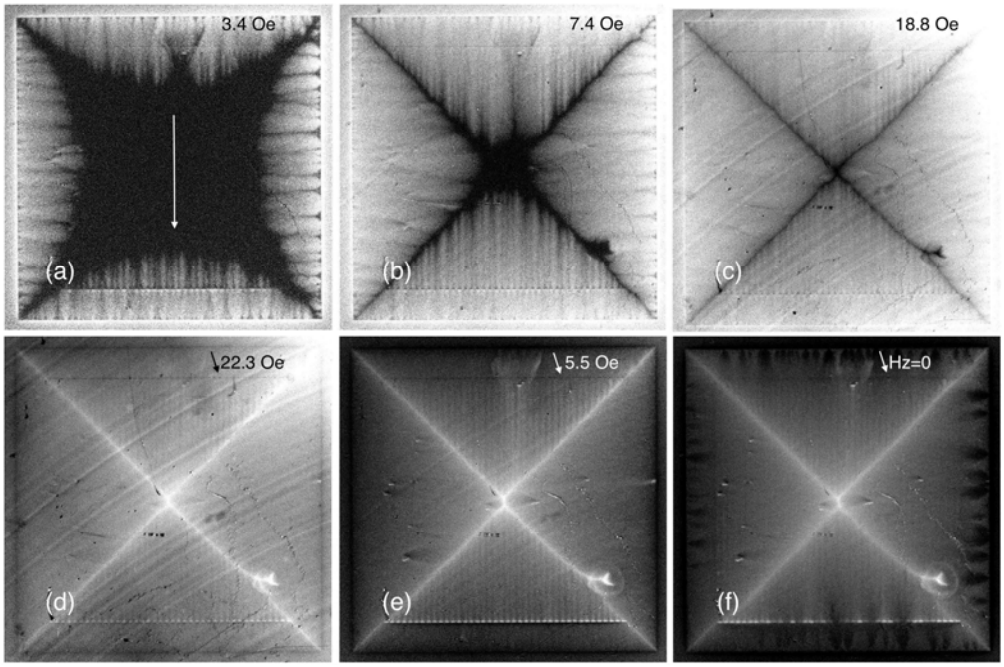

Fig.10 Normal flux entry (a-c) and exit (d-f) in the sample with longitudinally polarized stripes at 7K. The flux streaks from the top and bottom Py pattern sides follow the stripe periodicity with maximum B_z at the inter-stripe gaps. The flux entry across the stripes (from left and right sides of the Py pattern) lacks periodicity. The anisotropy of the exiting vortex dynamics yields short vertical SCT line in the sample center as shown in (e)-(f).

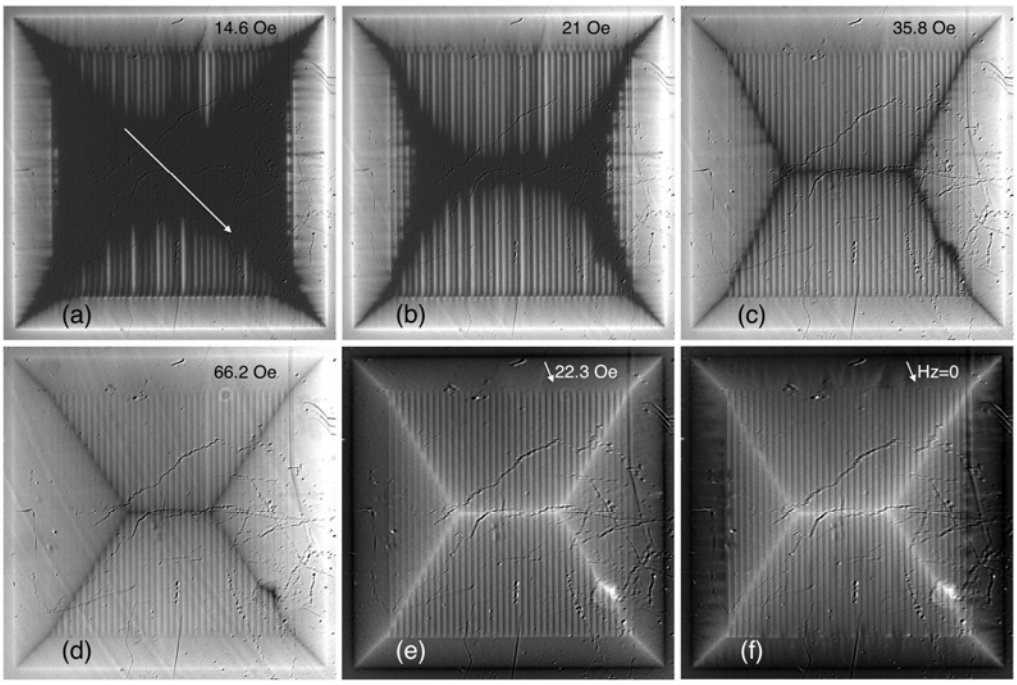

Fig.11 Normal flux entry (a)-(d) and exit (e)-(f) in the sample with diagonally polarized stripes. T=4K. The in-plane field direction is shown by arrow in (a).

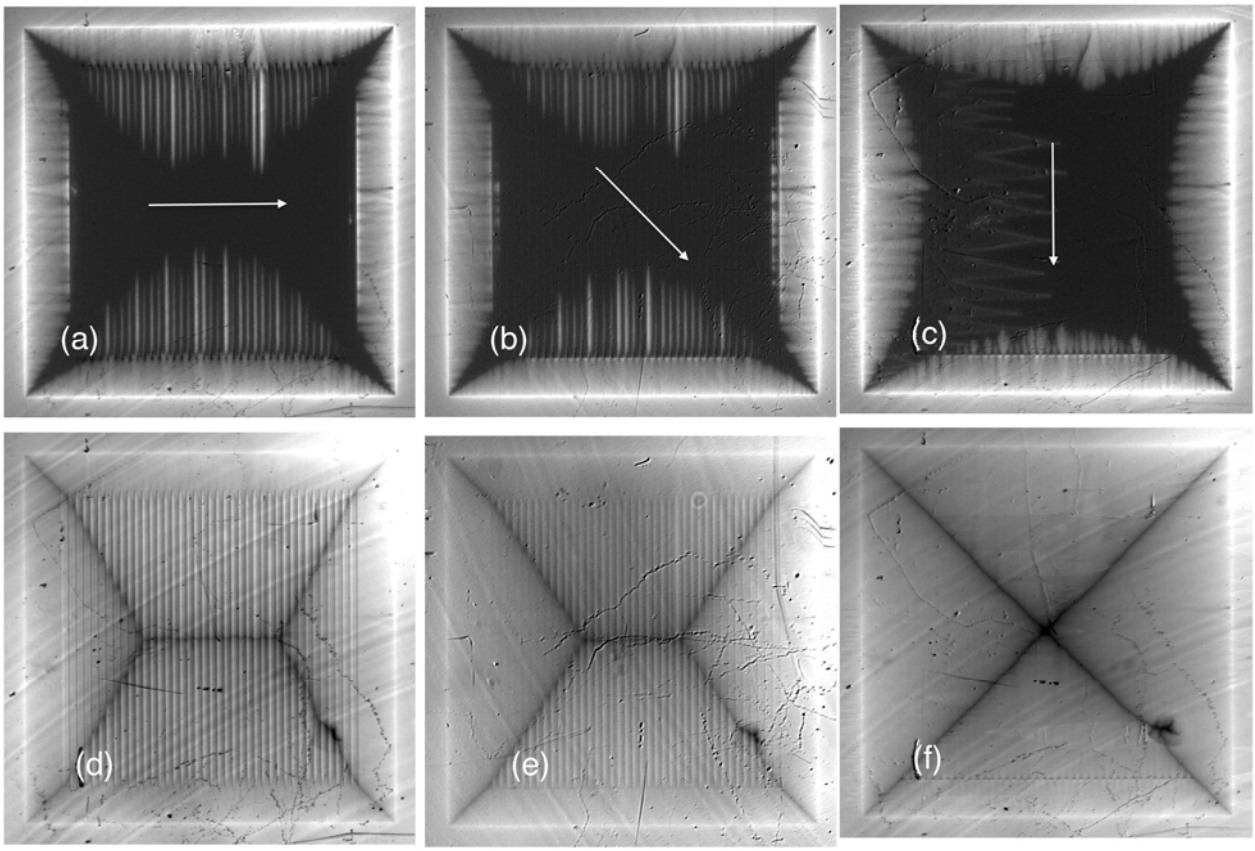

Fig.12 Comparison of the flux distributions at the initial stage of magnetization (top row, H_z=15.4 Oe) and in the total critical state (bottom row, H_z=66.2 Oe) for three different polarization directions of the Py stripe obtained at T=4K. Directions of the in-plane field are shown in the top pictures by white arrows.